CrossMark

RESEARCH PAPER

Optimization of welding loads with narrow groove and application of modified spray arc process

Dirk Schroepfer[1] · **Arne Kromm[1]** · **Thomas Kannengiesser[1]**

Abstract Current efforts for lightweight design result in a growing application of high-strength fine-grained structural steel in modern constructions, e.g. mobile cranes, with yield strength from 960 MPa. The design of welded structures and welding processes becomes more challenging with increasing material strength and elastic ratios. High residual stresses are able to diminish lifetime, load capacity and component safety and should be avoided. Recent analyses have shown strong influences of heat control and restraint of the weld due to arising reaction stresses, superimposing with local residual welding stresses. Modern inverter technologies allowed the development of numerous modified spray arc processes driven by power source manufacturers, which provide virtually similar features and several benefits, enabling welding of narrower seams with reduced weld volumes and total heat inputs. This research focuses on welding loads due to modified weld seams. The global reaction forces and moments and their superposition with local residual stresses in welded components due to external shrinkage restraints were investigated using a special testing facility and XRD. The restraint intensity, weld seam geometry and welding process were varied for statistical evaluations of resulting welding loads. When welding under restraint, a reduction of the weld seam volume causes significantly lower reaction stress levels.

Keywords (IIW-Thesaurus) Residual stresses · MAG welding · Restraint · High-strength steels · Process parameters

1 Introduction

Presently, the use of high-strength fine-grained structural steel in modern steel constructions increases. Similar to the mobile crane industry, these steels are applied in many structures to reduce the self-weight due to smaller possible wall thicknesses [1]. Moreover, an enhanced efficiency of energy and resources can be reached during production and service of high-strength steel components. Modern mobile cranes are primarily made of steels with yield strength from 960 MPa [2]. However, the increasing material strength involves a more demanding design of welded structures. A more challenging welding processing is also a result of closer technical boundaries, e.g. $\Delta t_{8/5}$-cooling times, to meet the requirements for the mechanical properties of the weld seam [3, 4].

Furthermore, the formation of high welding-induced residual stresses has to be avoided, especially in high-strength steels, because of high elastic ratios [5]. Besides an increased cracking risk, high tensile residual stresses are able to diminish the lifetime, the load capacity and the component safety [6, 7]. Recent numerical and experimental analyses showed a strong influence of the heat control and the rigidity of the weld on the global welding loads and local residual stresses in the weld seam [8–16]. Global reaction stresses and moments may arise while welding and cooling due to an external shrinkage restraint of the welded structure [17]. These multi-axial welding loads superimpose with local residual stresses in the weld seam. The superposition may lead to critical tensile stresses

✉ Dirk Schroepfer
dirk.schroepfer@bam.de

Arne Kromm
arne.kromm@bam.de

Thomas Kannengiesser
thomas.kannengiesser@bam.de

[1] Bundesanstalt für Materialforschung und -prüfung (BAM), Unter den Eichen 87, 12205 Berlin, Germany

🍃 Springer

in the weld and contiguous weld zones especially in welds with high restraint conditions, e.g. repair welds [18].

Today's most important joining process of high-strength structural steels is gas metal arc welding (GMAW). In high-strength steel welding, the transitional arc process (see Fig. 1) is common [11, 19], which is the transitional process working range between short and spray arc. This is due to a convenient ratio of deposition rate and heat input, especially for the low cooling times that have to be achieved in high-strength steel welds. A higher deposition rate and, therefore, higher efficiency of welding manufacturing could be achieved using spray arc processes. In order to limit the heat input and the deflection of those arcs, the arc length and the voltage of these spray arcs have been reduced to a minimum. However, this minimisation is limited by stable spray arc conditions, avoiding excessive spattering.

Therefore, GMAW power source manufacturers developed numerous modified spray arc (mod.SA) processes owing to the evolution of modern inverter technologies [19]. These welding processes enable very short spray arcs and low welding voltage, which is achieved due to an advanced control of the welding current by an event-driven adjustment of the current upslope. With that, a prevention of severe short circuits and of excessive spattering from the weld pool has been achieved. Each variant of the modified spray arc processes of the different producers of welding machines has a differerent brand name, but features virtually the same characteristics and further economic benefits [20]. Due to a high plasma pressure and a very short arc, an improved directionally stable arc with deep fusion penetration and good root fusion is reachable.

Thus, increased contact tube distances (stick out up to 40 mm) are possible, which allow significantly reduced groove angles and remarkable savings of filler material, welding time as well as weld preparation and weld finishing compared to standard arcs. Furthermore, a lower total heat input causes reduced distortions and leads to less setup times. But especially in context with a changed seam geometry, smaller weld volumes and total heat input, considerably reduced welding stresses are attainable; see Fig. 1. Moreover, a decreased bending moment is achievable due to the more symmetric weld build-up. Hence, the load capacity of high-strength steel structures could be increased. Recent researches proved the general weldability of high-strength steels with the modified spray arc process [21]. Investigations regarding the influence of this modern welding process along with smaller groove angles on the residual stresses and the overall stressing in welded components are missing.

Therefore, this research focuses on the welding loads due to modified weld seam geometries. In particular, the global reaction forces and bending moments in welded components due to an external shrinkage restraint were analysed. Weld tests were taken out with free shrinking specimens of high-strength steel S960QL and under defined restraint in a special in-house developed testing facility. The results are expected to help making quantitative forecasts of magnitudes and locations regarding residual stresses. In contrast, currently residual stresses are considered by across-the-board assumptions to the amount of the yield strength in high-strength steels. Furthermore, a reduction of welding stresses by an optimized application of the modified spray arc could be derived.
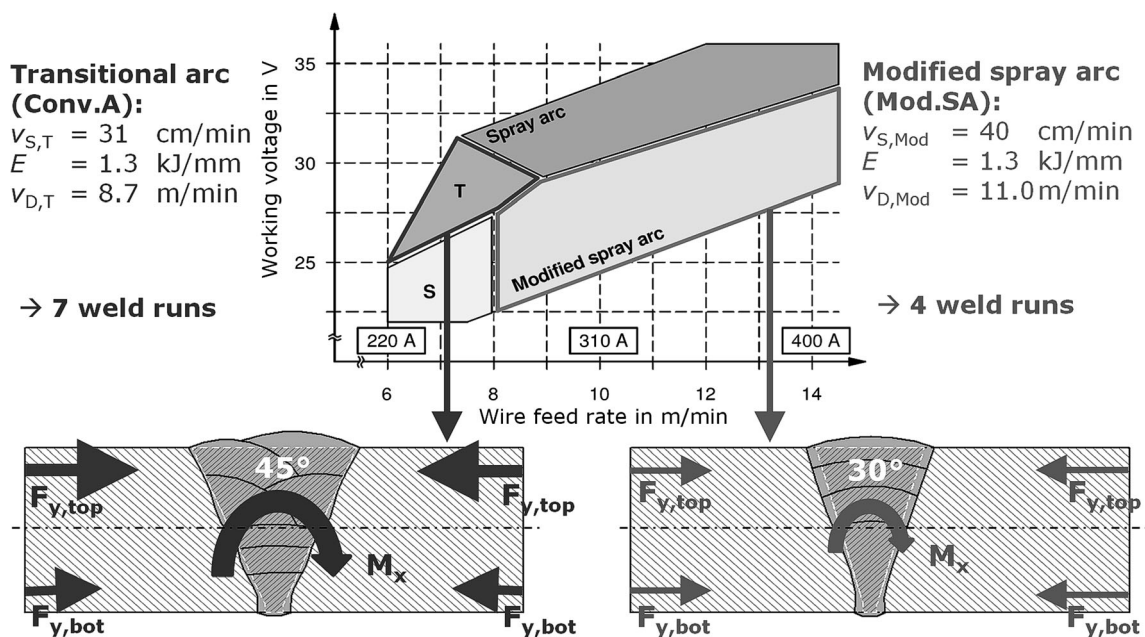

Fig. 1 Diagram of the process working ranges according to [19] and schematic of welding stress evolution. *T* transitional arc, *S* short arc, *vS* welding speed, *E* welding heat input, *vD* wire feed rate, *Fy* reaction force transverse to weld, M_x bending moment around the weld seam axis

Table 1 Chemical compositions (spark emission spectroscopy, Fe balanced) and mechanical properties of the test materials

Element (%)	C	Si	Mn	Cr	Mo	Ni	V	Nb	Ti
Base material (EN 10025-6, S960QL [22])									
	0.16	0.23	1.24	0.20	0.61	0.05	0.040	0.015	0.003
Filler material (EN ISO 16834-A-G 89 6 M21 Mn4Ni2CrMo [23])									
	0.08	0.87	1.84	0.35	0.57	2.23	0.005	–	0.070
Property		$R_{p0.2}$ in MPa		R_m in MPa		A_5 (%)	Av at − 40 °C (J)	HV10	
Base material									
(mechanical testing)		1035		1050		17	96	332 ± 8	
Filler material									
(producer testing report)		938		980		15	62	354 ± 7	

2 Experimental

Weld tests were performed using the high-strength fine-grained structural steel S960QL in 20-mm plate thickness according to EN 10025-6 [22] with a similar high-strength solid wire EN ISO 16834-A-G 89 6 M Mn4Ni2CrMo [23]. Table 1 shows the chemical composition and the mechanical properties of the materials. The automated multilayer GMA welds were performed at the V-groove butt joints. The welding parameters are given in Fig. 2. The parameter variation was selected within design of experiments (DoE) for the investigation of the effects of the welding process, the seam geometry and the restraint condition; see also Fig. 5. The groove angle was varied between 30° and 45°, which results in cross-sectional areas of A = 126.1 to 189.5 mm². The 30° groove angle was welded with the modified spray arc. Within the 45° V-butt joints, the transitional arc (Conv.A.) was applied.

The transitional arc is currently the typical welding process in high-strength steel fabrication (the mobile crane industry). Every welding process and seam

geometry was welded with specimens under free shrinkage (weld test nos. 1, 4 and 7). All the other weld tests were accomplished with specimens clamped into the 2-MN-testing facility [11, 12]; see Fig. 3. This testing facility allowed defined restraint conditions and a synchronous online measurement of the reaction forces and moments while preheating, welding and cooling.

For quantification and comparison of restraint conditions, especially between test setups and real component welds, the restraint intensity concept was established by Satoh [24]. The restraint intensity transverse to the weld R_{Fy} is the spring rigidity of the surrounding structure towards the weld seam based on the seam length L_W. With a constant system restraint of the testing facility and the same clamping length, the restraint intensity of the test setup at the 2-MN-testing facility was varied via the weld length from 3 kN(mm·mm)$^{-1}$ (L_W = 200 mm) to 4 kN(mm·mm)$^{-1}$ (L_W = 100 mm). The achieved restraint intensities are typical values of welding applications in the mobile crane industry [11].

The welding process conditions were observed in all weld tests. The welding current, voltage and speed were measured to control the heat input. The thermal cycle was monitored using type-K thermocouples (preheat and interpass temperature). The temperature on the weld seam was measured via a two-colour pyrometer (measuring range 350 to 1300 °C). The $T(t)$-curves allowed the determination of the $\Delta t_{8/5}$-cooling times to ensure production-relevant process conditions. Furthermore, the free shrinking samples were tested regarding their mechanical and technological properties.

X-ray diffraction (XRD) was used to analyse the local residual stresses transverse to the weld via the $\sin^2\Psi$-method. This was performed at the free shrinking weld test specimens and at the clamped ones directly in the 2-MN-testing facility to investigate the superposition of the global welding loads and local residual stresses (Fig. 3). The measurements were taken out in the centre of each specimen at the top surface of the base material, the heat-affected zone (HAZ) and weld metal; see Fig. 4.

Welding process	Mod.SA	Conv.A
Welding current	320 A ± 10 A	265 A ± 10 A
Welding voltage	28.7 V ± 0.1 V	26.5 V ± 1 V
Welding speed	400 mm/min to 420 mm/min	327 mm/min
Wire feeding speed	11 m/min	8.7 m/min
Preheat / interpass temperature $T_{p/i}$	100 °C	
Heat input E	1.3 kJ/mm	
Seam geometry and build-up sequence		
Cross-sectional weld area A in mm²	126.1 161.8 189.5	
Weld runs	4 6 7	

Fig. 2 Welding parameters and variation according to DoE (parameter matrix, see Fig. 5)
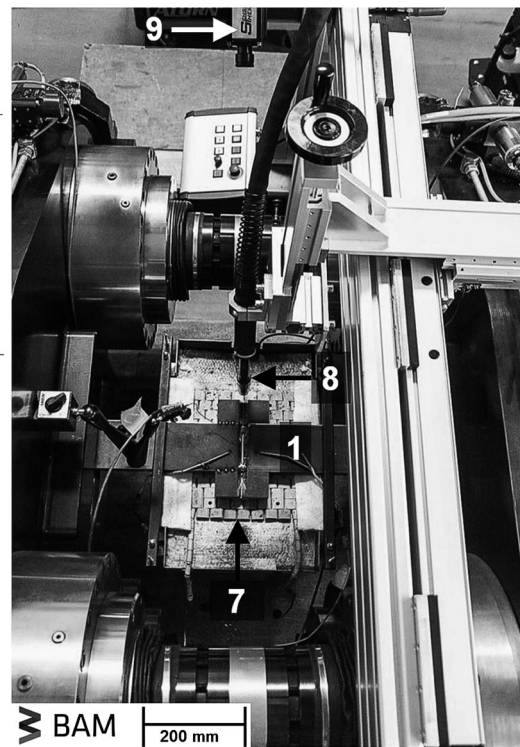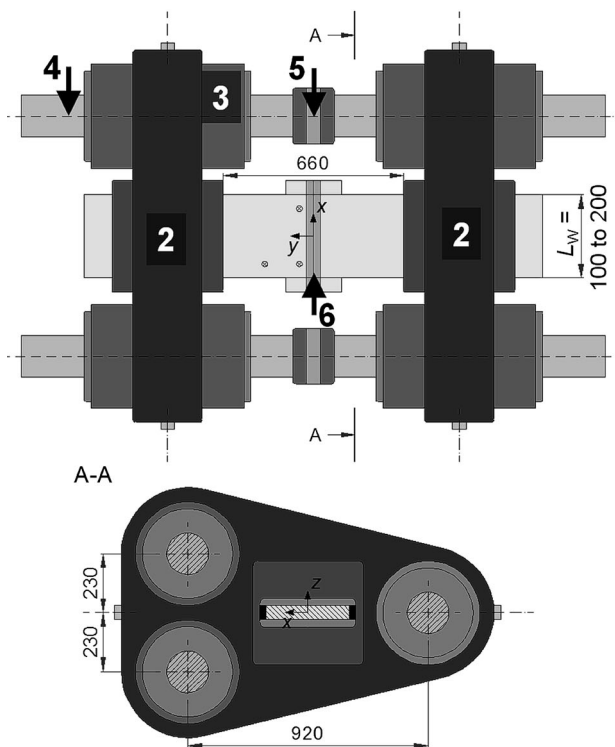
Fig. 3 Schematic and overview picture of the 2-MN-testing facility with specimen and weld test equipment. *1* specimen with attached thermocouples, *2* test desks with hydraulic clamping (500 bar), *3* hydraulic cylinder (200 bar), *4* piston rod, *5* load cell, *6* weld seam with start and end tabs, *7* heating mat, *8* GMAW torch, *9* two-colour pyrometer

3 Results

Figure 5 presents the $\Delta t_{8/5}$-cooling times and welding results for the weld tests with varied welding process and groove angle. The recommended $\Delta t_{8/5}$-cooling time range for this steel grade was achieved, and the mechanical properties of the weld met the requirements. Also, the radiographic examinations, ultrasonic testing and microstructure analysis showed no irregularities.

3.1 Global load analysis
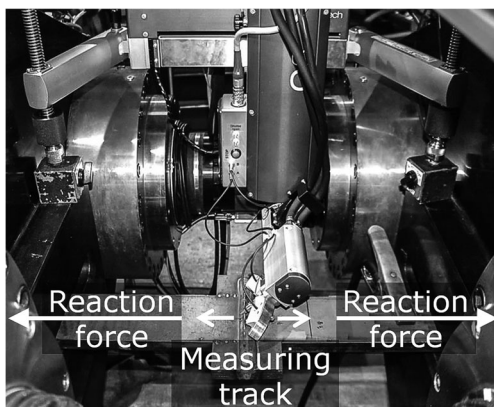
- Reaction forces

Fig. 4 Residual stress analysis of clamped specimens

In Fig. 6, the reaction force $F_y(t)$ and temperature $T(t)$ monitored in weld test no. 2 using the 2-MN-testing facility are presented.

The reaction force becomes compressive during preheating of the tack-welded specimen. The welding of the root leads to a first reaction force build-up. The further shrinkage of the solidified inserted weld metal while the root weld is cooling down to interpass temperature $T_i = 100$ °C produces

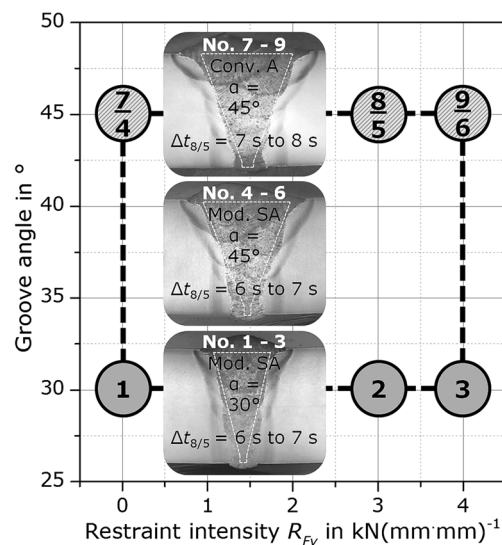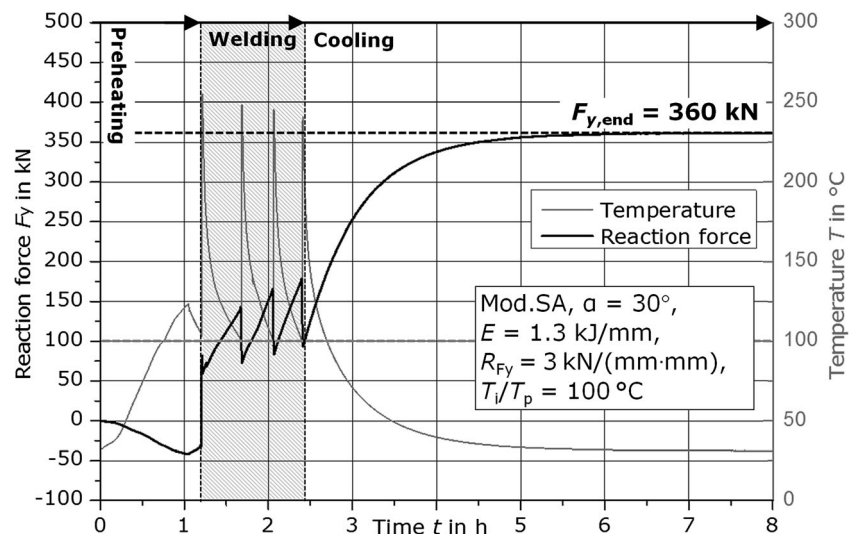**Fig. 5** Welding results and $\Delta t_{8/5}$-cooling times within the DoE parameter matrix ($R_{Fy} = 0$ kN(mm·mm)$^{-1}$ means welding under free shrinkage)

Fig. 6 Reaction force $F_y(t)$ and temperature $T(t)$ for weld test 2 under defined restraint $R_{Fy} = 3$ kN(mm·mm)$^{-1}$ in the 2-MN-testing facility (S960QL, heat input $E = 1.3$ kJ/mm, four runs, working temperature $T_{p/i} = 100$ °C)

transversal shrinking forces with a first maximum of $F_y = 140$ kN. The local heat input due to the welding of the next layer initiates a force reduction. After that, cooling to T_i causes a reaction force increase again. At every weld sequence, a similar behaviour of the reaction force is observable. However, the amplitude of the force increases with every weld run. The cooling of the complete weld to ambient temperature leads to a maximum of the reaction force of approx. $F_{y,end} = 360$ kN. Figure 7a shows the comparison of the reaction force build-up $F_y(t)$ for the two weld tests under restraint of $R_{Fy} = 3$ kN(mm·mm)$^{-1}$ with different welding processes and adopted groove angles. As the two $F_y(t)$ graphs show the same qualitative behaviour, the specimen with 30° groove angle welded with the mod.SA has an approx. 40% shorter total welding time due to the reduced seam volume, which leads to four necessary weld runs instead of seven at the 45° groove angle weld. Although the root of the mod.SA weld shows a higher amplitude of the reaction force because of the increased inserted load bearing section, the reaction force before and after cooling to ambient temperature is about 40 kN lower. Therefore, the reduced overall heat input and the smaller volume of the inserted weld metal results in a decrease of the end reaction force of about 10%.

- Normal reaction stresses

In order to compare the results considering the different restraint intensity varied via the weld length L_W, the determination of the reaction stress is necessary.

Therefore, Fig. 7b shows the corresponding reaction stress build-up according to the weld tests of Fig. 7a. Using micrographs of the cross sections, the transient load bearing height (transverse section) of the weld was measured. The calculation of the reaction stress build-up $\sigma_y(t)$

as normal stress is based on this transient height $H_{Layer}(t)$ and reaction force $F_y(t)$. Comparing both $\sigma_y(t)$ graphs, also the different behaviour while welding reveals. The insertion of the higher load bearing section of the root weld due to the decreased seam volume leads to approx. 30% lower reaction stress after cooling to $T_i = 100$ °C. As a result, the following sequences are welded at a significant lower reaction stress level. Finally, Fig. 8 shows the results of the end reaction stress of all experiments welded under restraint. The model quality R^2 of the regression is over 99%. Due to the small scatter of the results, both the restraint intensity R_{Fy} and cross sectional weld area A have a significant effect on the normal stress as a result of the welding-induced load. Regarding the selected parameter matrix, the effect of the restraint intensity is somewhat higher.

- Bending moments

Due to the three-dimensional configuration of the hydraulic cylinder system of the 2-MN-testing facility, besides the normal stresses, also the bending moments and stresses could be measured; see Fig. 3.

Bending moments in a weld occur when angular contraction while welding and cooling is restrained. Figure 9a shows the build-up of the so called reaction moment M_x with regard to the neutral axis of the plate. The calculation of M_x is based on the measured differences between the upper and the lower load cell on both the left side piston rods of the hydraulic cylinder system. It also considers the actual load bearing height, which influences the lever arm and, hence, the difference of measured forces. On that account, the reaction moment is not influenced by the preheating of the tack-welded specimen. The welding

Fig. 7 Comparison of the reaction force build-up $F_y(t)$ (**a**) and reaction stress build-up $\sigma_y(t)$ (**b**) for weld tests with different welding processes and adopted groove angles
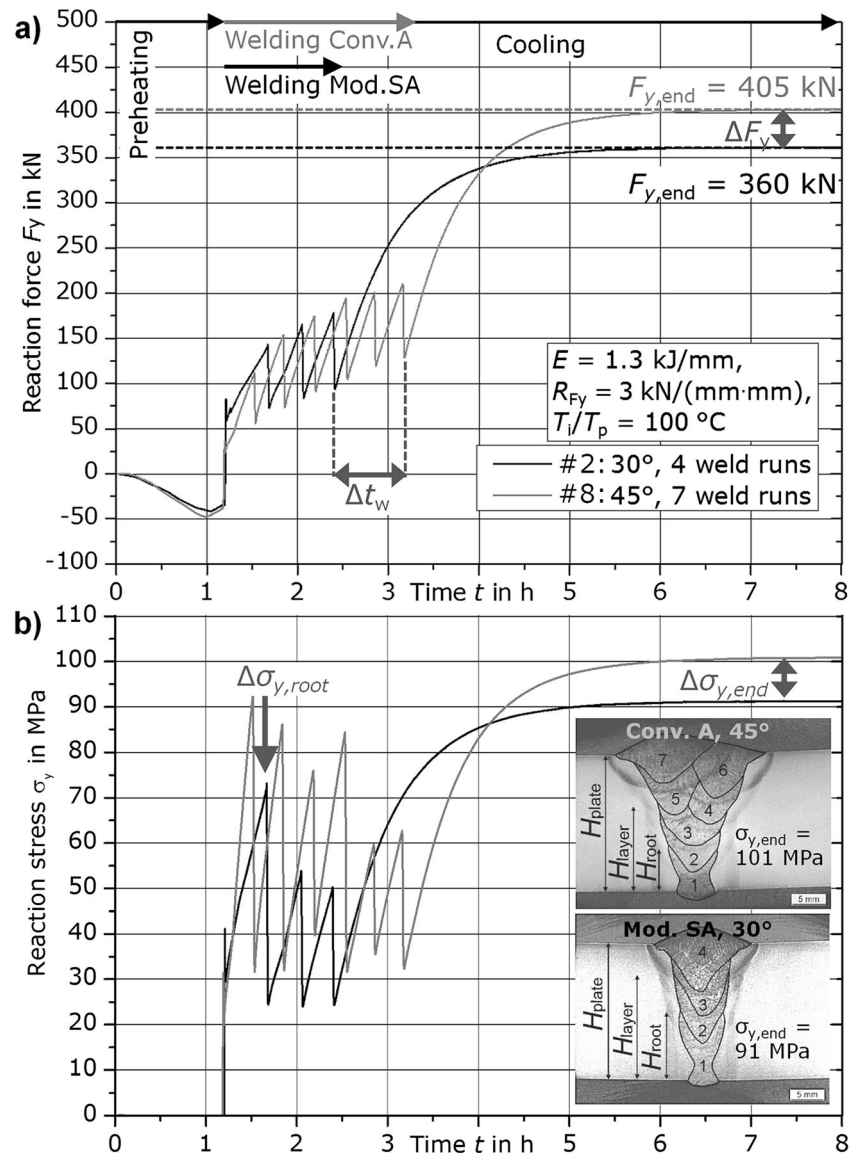
of the root initiates a first increase of the restrained angular contraction due to the asymmetric shrinkage of the already inserted solidified weld metal. The bending moment increases appreciably while cooling to interpass temperature to a first maximum of approx. $M_x = 0.8$ kNm. The heat input on the top side of the root weld of the next layer almost eliminates this first bending moment build-up. Cooling to interpass temperature again leads to an increase of the restrained angular contraction of about $M_x = 0.6$ kNm. It can be observed that this behaviour repeats at every weld sequence. The amplitude of the reaction moment decreases with almost every weld run with an increasing mean level. However, the welding of the fourth weld run causes a less reaction moment decrease and a higher increase while cooling to interpass temperature up to $M_x = 1.0$ kNm. Two reasons clarify this divergence to the other weld runs. Primarily, the fourth weld

run is the first one welded above the neutral axis of the specimen. The first layer above the neutral axis has the largest impact on the restrained angular distortion build-up. Secondly, this weld run is inserted asymmetrically into the seam, which inhibits an effective reduction of the reaction moment from the previous layer and does not add additional load bearing weld height; the section modulus does not increase. In addition, a more inhomogeneous heat input with a higher eccentricity is effected [17].

The fifth weld run reduces the bending moment to $M_x = 0.3$ kNm. Subsequent cooling leads, finally, to a bending moment accumulation up to $M_x = 0.95$ kNm.

A comparison of the bending moment build-up in Fig. 9b shows a qualitatively equal, but quantitatively completely different development for the mod.SA weld with a 30° groove angle. Although the first amplitude of
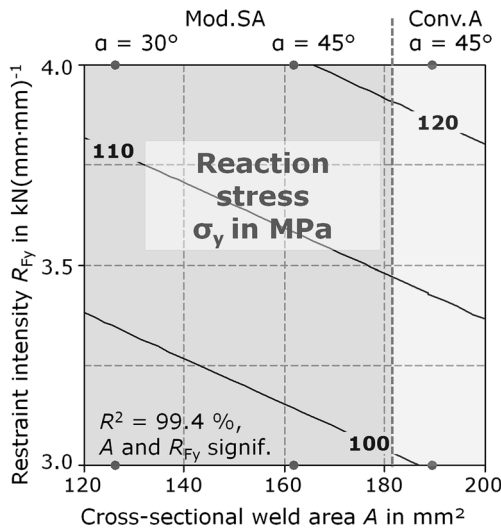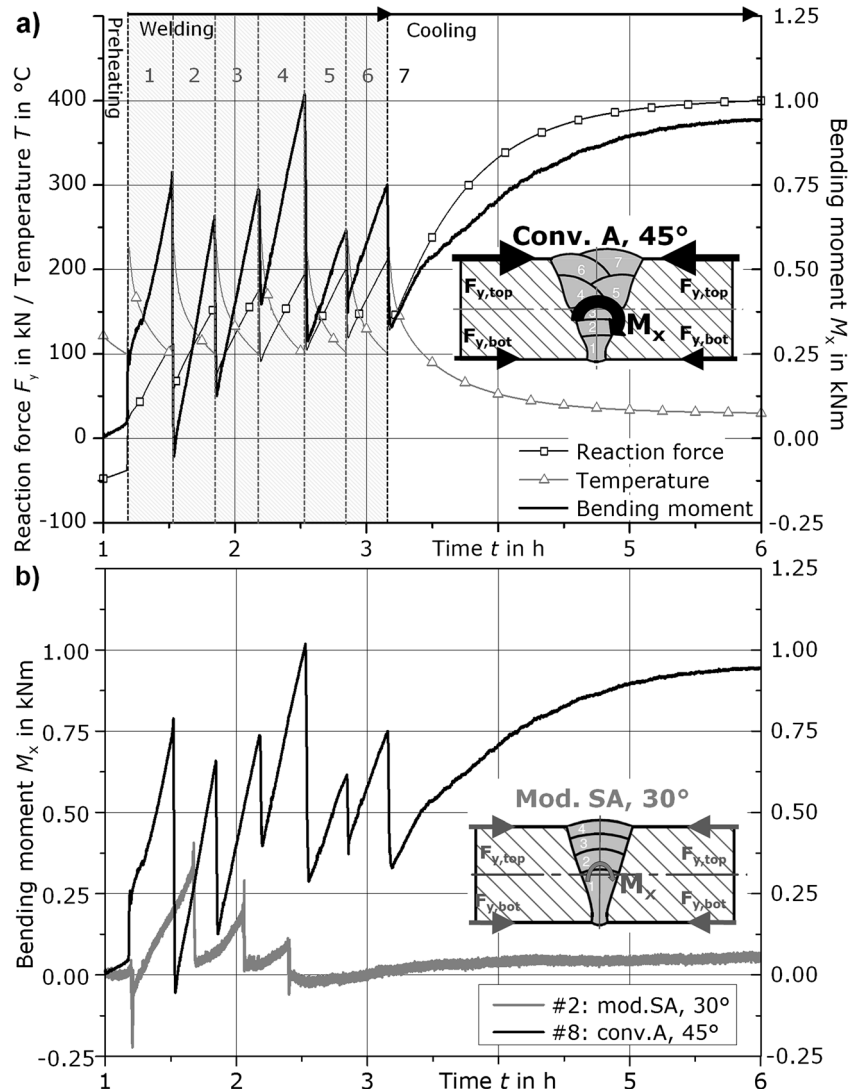
Fig. 8 Contour plot of the reaction stress σ_y after cooling to ambient temperature of the restraint welds versus restraint intensity R_{Fy} and cross sectional weld area A (standard deviation of regression model is $S = 1.1$ MPa)

the bending moment due to welding and cooling of the root and welding of the second layer is the highest with a maximum of 0.4 kNm, the welding of all following layers causes decreasing amplitudes of the bending moment and an almost constant mean level. Subsequent cooling to ambient temperature causes virtually no further reaction moment build-up. The insertion of a load bearing height on the amount of the neutral axis height during root welding in combination with a more symmetric build-up of the weld and a less eccentric seam geometry is obviously beneficial to either prevent a high angular distortion or, if restrained, to diminish the bending moments [17].

Finally, the statistical evaluation of the results (regression analysis) of the bending moments after cooling to ambient temperature showed a strong effect of the cross-sectional weld area A; see Fig. 10. The regression exhibited a good model quality of about $R^2 = 83\%$ with one significant factor, A. The restraint intensity R_{Fy} had no significant influence on the bending moment.
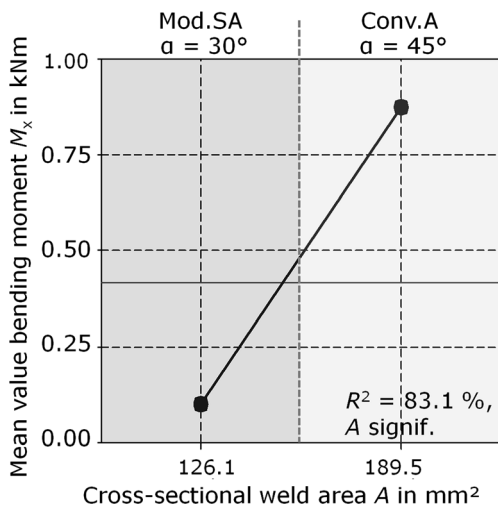
Fig. 9 Build-up of the bending moment $M_x(t)$ of test no. 8 (conv.A, 45°, seven runs, $R_{Fy} = 3$ kN/(mm.mm), **a** compared to reaction force $Fy(t)$ and temperature $T(t)$ and **b** compared $M_x(t)$ of test no. 2 (mod.SA, 30°, four runs, $R_{Fy} = 3$ kN/(mm.mm))

Fig. 10 Main effects plot of the bending moment M_x after cooling to ambient temperature versus the cross-sectional weld area A

3.2 Local residual stress analysis

- Effect of welding process and seam geometry

Local restraint stresses in the weld are due to process conditions and material behaviour. In case of Fig. 11, a superposition of the local restraint stresses and the reaction stresses is shown. The stresses were measured in direction of the shrinkage restraint in the weld test specimens clamped into the 2-MN-testing facility. Both σ^{rs}_y profiles show typical distributions for a steel with an undergoing phase transformation during cooling [8]. The residual stress profile in the weld test no. 9 is more asymmetric and broader compared to that of the weld test no. 3 because two cap beads were necessary. The residual stresses in the last cap bead are the highest at about 350 MPa.
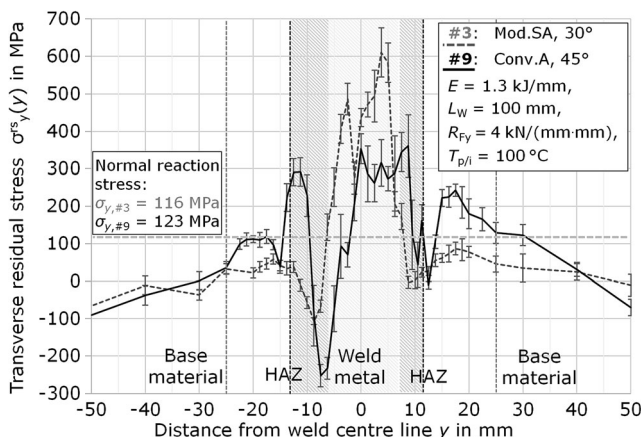
The residual stresses in the weld metal of test no. 3 show maximum values of up to 600 MPa a few millimetre next to the weld centre line. Obviously, the deeper penetration of the mod.SA produces higher residual stress peaks at the surface of the weld metal. These are a result of the larger heated volume, which involves a higher inhomogeneous shrinkage and restraint stresses, respectively. The corresponding temperature gradients in plate thickness direction are capable to produce additional tensile stresses at surface of the weld due to inhomogeneous phase transformation in between the core area of the weld and the surface and border areas. Furthermore, effects from quenching, tempering and phase transformation lead to minima of the residual stress profile in the weld metal of weld test no. 9 down to −250 MPa [8].

Other minima of the transverse residual stresses reveal in both weld tests next to the weld transition at the HAZ. In the further course of the HAZ to the base material, secondary maxima are obvious, before the residual stress level reaches a basic level in the parent plates. By comparison of both σ^{rs}_y profiles, higher secondary maxima reveal in the HAZ of the conv.A weld.

- Effect of restraint

For a comparison of the influences on the residual stresses of the test specimen, Fig. 12 shows residual stress distributions $\sigma^{rs}_y(y)$ welded and measured in different restraint conditions. Both welding processes reveal residual stress levels on the surface of the weld metal, which are relatively independent from the restraint condition. The maxima of the mod.SA weld are from approx. 500 to 600 MPa and of the conv.A welds from 350 to 450 MPa due to a less weld penetration. However, by comparison of the residual stress level at the HAZ, a high effect of the restraint condition reveals for the conv.A welds. The increase of the residual stress level in the HAZ is
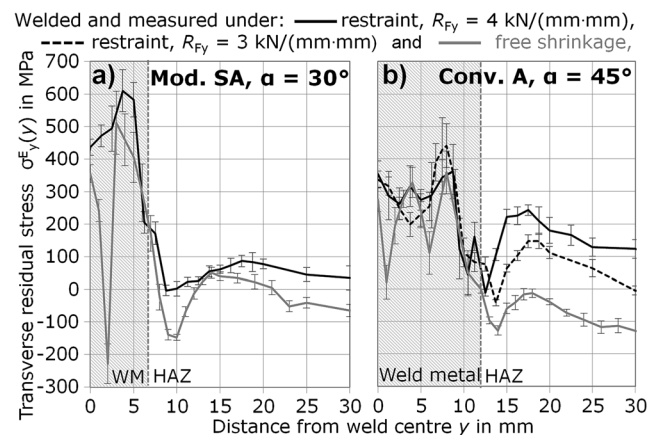

Fig. 11 Comparison of transverse residual stress distributions $\sigma^{rs}_y(y)$ for two different welding processes with adopted groove angles, measured with applied restraint in the 2-MN-testing facility on the *top surface* of the welds

Fig. 12 Comparison of transverse residual stress distributions $\sigma^{rs}_y(y)$ on the *top surface* of the welds for two different restraint conditions in specimens welded with **a** mod.SA and 30° groove angle and **b** conv.A and 45°

proportional to the measured normal reaction stresses for the mod.SA weld with 30° groove angle, but disproportionately high in the conv.A welds with 45° groove angle; compare Fig. 8.

4 Discussion of the welding loads

As shown, the higher welding stresses in the HAZ of the conv.A welds cannot be described by the global normal welding loads. However, the results correlate with the bending moments, which are caused by differences between the reaction force of the top and the bottom of the welds. As a consequence, the reaction stress at the top of the weld has to be higher if a positive bending moment occurs; see Fig. 13. With respect to this inequality of the global reaction stress over the transverse section of the weld, the resulting total reaction stress (Table 2) of the weld top site can be calculated by Eq. 1 [9]:

$$\sigma_{y,top} = \sigma_{y,end} + \sigma_{Mx} = \frac{F_y}{A} + \frac{M_x}{W_x} \qquad (1)$$

Table 2 shows the results of the reaction stresses on the top side of the weld for all specimens welded in the 2-MN-testing facility.

Finally, the statistical evaluation of the reaction stresses on the top side of the plate $\sigma_{y,top}$ is shown in Fig. 14. The regression of these reaction stresses revealed a high model quality of approx. $R^2 = 92\%$ and significant effects for both the restraint intensity R_{Fy} and cross-sectional weld area A. This result is in good agreement with the residual stress levels located in the range of the secondary stress maximum in the HAZ of each weld; compare Fig. 12. The maximum values are corresponding to a high degree with the reaction stresses at the plate top side. At the same restraint condition, the reaction stresses on top of a weld can be reduced by 50% using the mod.SA with an adopted seam geometry.

5 Conclusions

In the present study, beneficial effects of a new welding process, which permits narrower weld seam geometries,
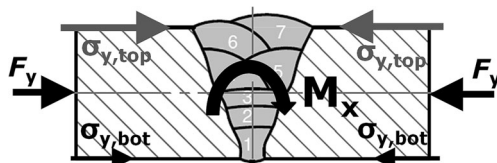

Fig. 13 Schematic of build-up of bending moments in restrained welds and resulting reaction stresses

Table 2 Resulting reaction stress on the top of weld of 2-MN-test specimens

Test no.	Welding process	Groove angle	$L_W = b$ (mm)	$\sigma_{y,end}$ (MPa)	M_x/W_x (MPa)	$\sigma_{y,top}$ (MPa)
2	Mod.SA	30°	200[a]	91	0.05/0.0133	95
3	Mod.SA	30°	100[b]	116	0.15/0.0067	139
5	Mod.SA	45°	200[a]	97	0.20/0.0133	112
6	Mod.SA	45°	100[b]	118	0.35/0.0067	171
8	Conv.A	45°	200[a]	101	0.95/0.0133	172
9	Conv.A	45°	100[b]	123	0.80/0.0067	243

Section modulus $W_x = b \cdot h^2 \cdot \frac{1}{6}, h = 20$ mm,

[a] $R_{Fy} = 3$ kN(mm·mm)$^{-1}$

[b] $R_{Fy} = 4$ kN(mm·mm)$^{-1}$

were investigated regarding welding loads. A variation of seam geometry, welding process and restraint condition was conducted. In free shrinking and component-related restrained multilayer GMA-weld tests with the high-strength steel S960QL, global and local welding stresses were analysed. From the results, the following conclusion can be drawn:

1) The mod.SA offers the opportunity to weld smaller seam volumes combined with less needed weld runs and decreased total heat input in compliance of the given $\Delta t_{8/5}$-cooling time range and required technological-mechanical properties.

2) In component-related welds with an external shrinkage restraint, mod.SA welding leads to significantly reduced reaction forces of about 10%.
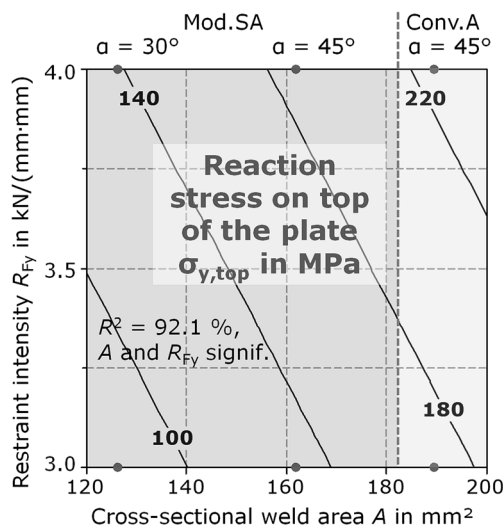

Fig. 14 Contour plot of the reaction stresses on the top side of the plate $\sigma_{y,top}$ after cooling to ambient temperature of the restraint welds versus restraint intensity R_{Fy} and cross-sectional weld area A (standard deviation of regression model is $S = 19.2$ MPa)

3) Due to a smaller groove angle, a higher load bearing weld height inserted during root welding causes reduced normal stresses while welding and a decreased reaction stress build-up while cooling to ambient temperature.

4) The build-up of the bending moment due to restrained angular distortion is greatly reduced in the 30° groove angle weld compared to that of the conventional welds. It is the result of a lower weld seam eccentricity combined with the effect of a root weld height above the neutral axis.

5) On the surface of the weld metal, higher transverse residual stresses revealed for the mod.SA due to a deeper weld penetration. On the other hand, in the critical HAZ, a disproportional high stress increase was observed for the conv.A welds for elevated restraint intensities.

6) Bending stresses as a result of bending moments in the weld are superimposed by normal reaction stresses. The calculated total reaction stresses on top of the welds due to positive bending moments are highly affected by the weld seam volume and the restraint intensity. At the same restraint condition, a reduction of the reaction stresses on the top side of the weld by 50% is achievable if the narrower weld seam geometry is applied.

7) From the manufacturers' point of view, the application of smaller groove angles is beneficial for a reduction of the profound critical stresses in the HAZ due to decreased global welding loads. A redistribution under service load of high tensile stresses in the HAZ that are caused by global welding loads might be suppressed, especially in high-strength steels due to the high yield strength. Also detrimental microstructures of the HAZ are able to diminish the component performance or lead to premature failure, particularly in combination with complex stress states. Oppositely, as a rule, high residual stress peaks on the surface of the weld metal are due to local volume changes. Along with a sufficient toughness of the weld metal, it is assumed that these shallow stress peaks vanish or relocate [25], respectively, during the first operating loads.

References

1. Guenther H-P (2005) Use and application of high-performance steels for steel structures. IABSE IVBH, Zürich

2. Hulka K, Kern A, Schriever U (2005) Application of niobium in quenched and tempered high-strength steels. Mater Sci Forum 500-501:519–526. doi:10.4028/www.scientific.net/MSF.500-501.519

3. Felber S (2008) Welding of the high grade pipeline-steel X80 and description of different pipeline-projects. Weld World 52:19–41. doi:10.1007/BF03266637

4. DIN EN 1011–2: Welding—recommendation for welding of metallic materials - Part 2: Arc welding of ferritic steels, 2001.

5. Shi G, Ban H, Bijlaard FSK (2012) Tests and numerical study of ultra-high strength steel columns with end restraints. J Constr Steel Res 70:236–247. doi:10.1016/j.jcsr.2011.10.027

6. Lu J (2002) Prestress engineering of structural material: a global design approach to the residual stress problem. In: Handb. residual stress deform. steel. pp 11–26

7. James MN (2011) Residual stress influences on structural reliability. Eng Fail Anal 18:1909–1920. doi:10.1016/j.engfailanal.2011.06.005

8. Nitschke-Pagel T, Wohlfahrt H (1991) The generation of residual stresses due to joining processes. In: Hauk V, Hougardy H, Macherauch E (eds) Residual Stress. - Meas. Calc. Eval. DGM Informationsgesellschaft mbH, ISBN: 3–88355–169-4, pp 121–133

9. Rhode M, Kromm A, Kannengiesser T (2012) Residual Stresses in Multi-Layer Component Welds. In: Trends weld. res. Proc. 9th Int. Conf. ASM International, ISBN: 1–62708–998-8, Chicago, Illinois, USA, pp 48–54

10. Schroepfer D, Kannengiesser T (2016) Stress build-up in HSLA steel welds due to material behaviour. J Mater Process Technol 227:49–58. doi:10.1016/j.jmatprotec.2015.08.003

11. Schroepfer D, Kromm A, Kannengiesser T (2015) Improving welding stresses by filler metal and heat control selection in component-related butt joints of high-strength steel. Weld World 59:455–464. doi:10.1007/s40194-014-0219-7

12. Lausch T, Kannengiesser T, Schmitz-Niederau M (2013) Multiaxial load analysis of thick-walled component welds made of 13CrMoV9-10. J Mater Process Technol 213:1234–1240. doi:10.1016/j.jmatprotec.2013.01.008

13. Boellinghaus T, Kannengiesser T, Neuhaus M (2005) Effects of the structural restraint intensity on the stress strain build up in butt joints. Math Model Weld Phenom 7:651–669

14. Satoh K, Nakajima H, Toyosada M (1972) Restraint intensity of weld joints in the structural members consisting of plates and stiffeners. IIW-Doc: X-660-72

15. Jiang W, Xu XP, Gong JM, Tu ST (2012) Influence of repair length on residual stress in the repair weld of a clad plate. Nucl Eng Des 246:211–219. doi:10.1016/j.nucengdes.2012.01.021

16. Jones WKC, Alberry PJ (1977) A model for stress accumulation in steels during welding. In: Residual stress. welded Constr. their Eff. The Welding Institute, London, 15–17 November 1977, Volume 1 - papers, pp 15–26

17. Masubuchi K (1980) Analysis of welded structures: residual stresses, distortion, and their consequences. Pergamon Press

18. Dong P, Hong JK, Bouchard PJ (2005) Analysis of residual stresses at weld repairs. Int J Press Vessel Pip 82:258–269. doi:10.1016/j.ijpvp.2004.08.004

19. H. Cramer, Baum L, Pommer S (2011) Überblick zu modernen Lichtbogenprozessen und deren Werkstoffübergängen beim MSG-Schweißen. In: DVS-Berichte 275. DVS Media GmbH, Düsseldorf, pp 232–237

20. Chen J, Schwenk C, Wu CS, Rethmeier M (2011) Predicting the influence of groove angle on heat transfer and fluid flow for new gas metal arc welding processes. Int J Heat Mass Transf 55:102–111. doi:10.1016/j.ijheatmasstransfer.2011.08.046

21. Heinze C, Pittner A, Rethmeier M (2013) Investigations of the weldability of high-strength fine-grained structural steels by application of modified spray arc processes. Final report of Research Project IGF 16.557N.

22. EN 10025–6: Hot rolled products of structural steels—Part 6: Technical delivery conditions for flat products of high yield strength structural steels in the quenched and tempered conditions, 2011.

23. EN ISO 14341: Welding consumables—Wire electrodes and weld deposits for gas shielded metal arc welding of non alloy and fine grain steels – Classification, 2011.

24. Satoh K, Ueda Y, Matsui S et al (1977) Japanese studies on structural restraint severity in relation to weld cracking. Weld World 15: 155–189

25. Zerbst U, Ainsworth RA, Beier HT et al (2014) Review on fracture and crack propagation in weldments—a fracture mechanics perspective. Eng Fract Mech 132:200–276. doi:10.1016/j.engfracmech.2014.05.012